ACS NANO

www.acsnano.org

ARTICLE

Liquid Crystal Coacervates Composed of Short Double-Stranded DNA and Cationic Peptides

Tommaso P. Fraccia*,‖ and Tony Z. Jia‖

Cite This: *ACS Nano* 2020, 14, 15071−15082

Read Online

ACCESS | Metrics & More | Article Recommendations | Supporting Information

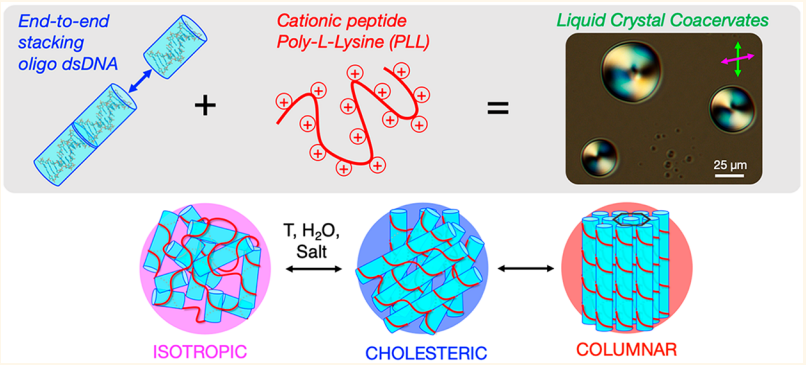

ABSTRACT: **Phase separation of nucleic acids and proteins is a ubiquitous phenomenon regulating subcellular compartment structure and function. While complex coacervation of flexible single-stranded nucleic acids is broadly investigated, coacervation of double-stranded DNA (dsDNA) is less studied because of its propensity to generate solid precipitates. Here, we reverse this perspective by showing that short dsDNA and poly-L-lysine coacervates can escape precipitation while displaying a surprisingly complex phase diagram, including the full set of liquid crystal (LC) mesophases observed to date in bulk dsDNA. Short dsDNA supramolecular aggregation and packing in the dense coacervate phase are the main parameters regulating the global LC-coacervate phase behavior. LC-coacervate structure was characterized upon variations in temperature and monovalent salt, DNA, and peptide concentrations, which allow continuous reversible transitions between all accessible phases. A deeper understanding of LC-coacervates can gain insights to decipher structures and phase transition mechanisms within biomolecular condensates, to design stimuli-responsive multiphase synthetic compartments with different degrees of order and to exploit self-assembly driven cooperative prebiotic evolution of nucleic acids and peptides.**

KEYWORDS: *phase separation, complex coacervation, liquid crystals, supramolecular assembly, membraneless organelles*

Phase separation is a ubiquitous process by which cells can segregate metabolites, compartmentalize reactions, or regulate genetic processes.[1,2] It has been suggested that phase transitions in liquid−liquid phase separated systems (LLPS) are involved in many pathologies.[3] As such, LLPS has been broadly investigated to gain a better understanding of the mechanisms driving the formation of membraneless organelles *in vivo*[4] and has been reproduced *in vitro* for applications in synthetic biology[5,6] and drug delivery[7] and proposed also as protocell models in origins of life research.[8−10] Complex coacervation is one major class of associative phase separation resulting from electrostatic interaction between oppositely charged polyelectrolytes. Herein, the most relevant for biology are nucleic acids (polymers,[11] oligomers,[12] or monomers[10]) and proteins (intrinsically disordered proteins,[13] peptides,[11] and amino acids[14]). The resulting coexisting phases include one dilute bulk phase and one condensed coacervate phase, enriched of both polyelectrolytes, but which still conserves liquid properties.[10,15] Such phase separation is fundamentally different from precipitation, as precipitates mostly are solid aggregates with an extremely low water content.[15] Polymer complexation and the resulting coacervation can generally be explained as the result of entropy gain due to counterion release from polymer binding.[16]

Received: June 18, 2020
Accepted: August 27, 2020
Published: August 27, 2020

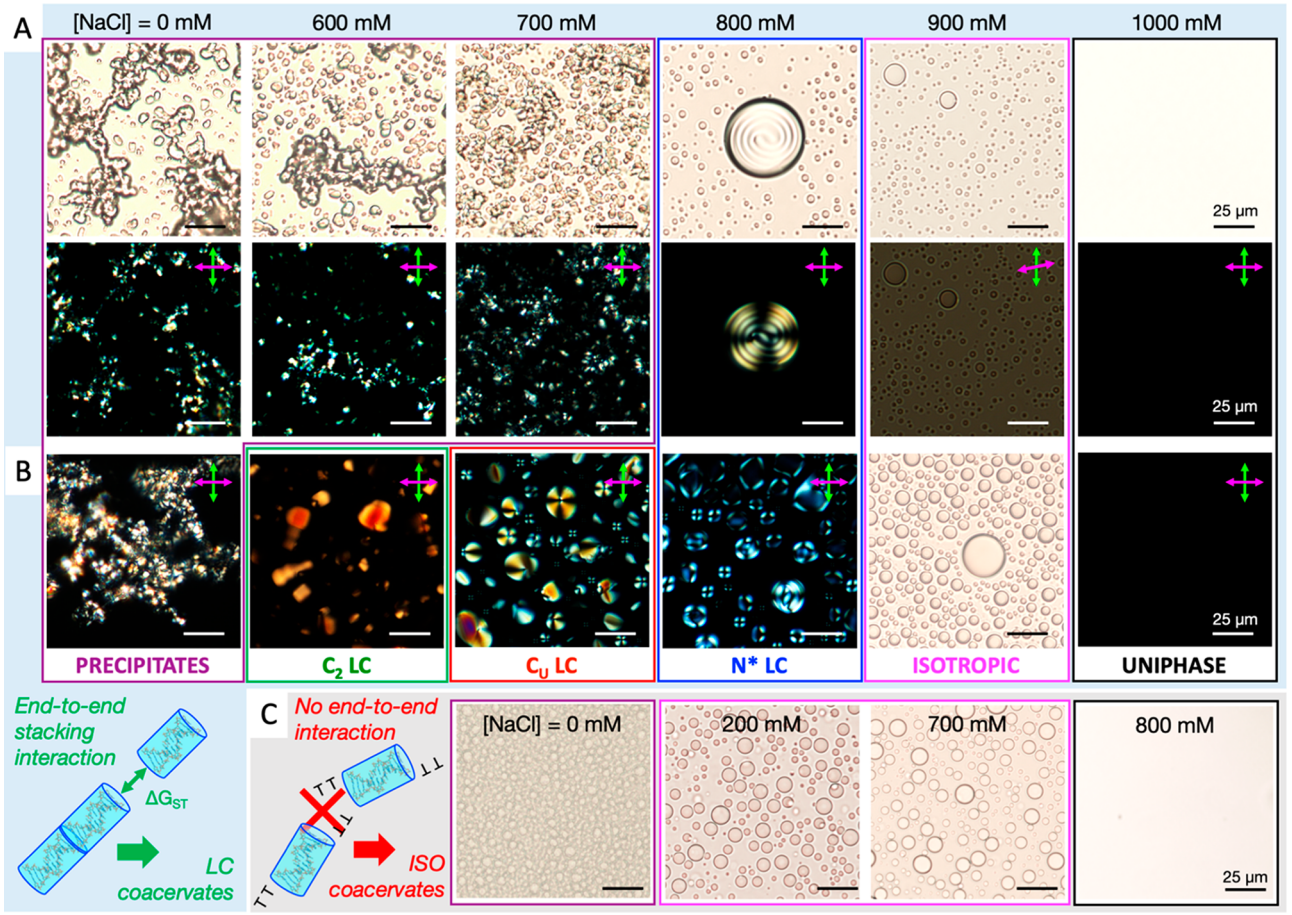

Figure 1. LC mesophases in dsDNA-PLL coacervates. (A) BFTOM (top) and PTOM (bottom) micrographs of rDD (5′-GCGCTTAAGCGC-3′) and PLL (MW = 30k−70 kDa), $N = P = 10$ mM ($Q = 20$ mM), assembly at varying [NaCl] at room temperature. (B) BFTOM and PTOM micrographs of LC-coacervate samples after annealing: heating to 90 °C followed by slow cooling ($\Delta T/dT < 5$ °C/min) back to room temperature. A sketch (bottom left) of the supramolecular aggregation of s-dsDNA blunt-ended duplexes driven by stacking which allows the formation of LC ordering inside the coacervate phase. (C) LC suppression and normal isotropic coacervate droplets were observed through BFTOM at 200 mM ≤ [NaCl] ≤ 700 mM by adding 3′-TT dangling-ends to s-dsDNA, which destabilizes the end-to-end interaction of the DNA duplexes. Scale bars are 25 μm. The green and magenta double-sided arrows indicate the orientations of the polarizer and analyzer, respectively.

Single-stranded DNA (ssDNA) and double-stranded DNA (dsDNA) generally show a dramatically different behavior when complexed with cationic peptides: the former favors coacervation, while the latter causes precipitation.[17] Indeed, polymer flexibility, hydrophilicity, and charge density are factors that govern the assembly and physical characteristics resulting from coacervation.[17,18] Single-stranded DNA is a flexible polymer, with persistence length ($l_p \sim 1$ nm) on the order of a few nucleotides, while dsDNA is a stiffer polymer with $l_p \sim 50$ nm, that is ∼150 base pairs.[19] Moreover, dsDNA has a higher charge density than ssDNA, ∼2.4 times greater, and is more hydrophilic than ssDNA, both being properties which disfavor coacervation.[17]

While generally coacervates of flexible ssDNA can be more readily assembled than dsDNA, the condensation of stiff dsDNA molecules by coacervation can potentially introduce more order to the unstructured liquid phase through the formation of liquid crystal (LC) phases.[20] LC phases can be produced in highly concentrated aqueous solutions of long dsDNA,[21] short dsDNA (s-dsDNA), and dsRNA oligomers[22−25] or even Watson−Crick pairs of deoxyribonucleotide triphosphates (dNTPs).[26] While the behavior of long NAs is typical for lyotropic LC systems of stiff rod-like molecules,[20] short oligomeric (<20bp) and monomeric NAs follow the assembly mechanism of chromonic LC systems:[27] LC ordering results from the amphiphilic nature of these molecules, for which hierarchical self-assembly steps triggered by base pairing and end-to-end $\pi-\pi$ stacking interactions of duplexed DNA fragments drive the formation of reversible linear aggregates which in turn order into LC phases.[22,25,26] Broad experimental studies on oligomeric dsDNA systems in bulk have shown the formation of isotropic (ISO), cholesteric (N*), uniaxial columnar (C_U), and higher-ordered columnar (C_2) LC mesophases, at increasing DNA concentration, [DNA], for various oligomers lengths, sequences, structural motifs, and system compositions.[22−26] Recent experiments showed that solutions of a 22bp dsDNA and poly-L-lysine (PLL) can form the N* LC phase within coacervate droplets at high salt concentrations, while at lower salt concentrations, only precipitates and gel-like particles were observed.[18] Moreover, a theoretical study of semiflexible polyanions and flexible polycations, using scale laws, has recently shown that the ISO−LC transition inside polymeric coacervates could be allowed for polyanions of sufficient rigidity.[28] However, based on structure alone, LC and coacervate systems appear to be incompatible: liquid coacervates can be considered as

https://dx.doi.org/10.1021/acsnano.0c05083
ACS Nano 2020, 14, 15071−15082

disordered globular clusters of flexible polymers capable of coiling upon themselves in order to stay liquid,[11,16] and LCs, on the other hand, although still fluid, are characterized by the long-range orientational or positional order of stiff dsDNA molecules.[21,22] Thus, given this apparent incompatibility, a deeper comprehension of the processes enabling LC assembly in coacervate droplets and of their inner structure is still lacking.

Here, we report the formation of LC-coacervates in mixtures of 12bp oligomeric s-dsDNA and PLL. Surprisingly, we observed the entire range of known mesophases (ISO, N*, C_U, and C_2) observed to date for bulk s-dsDNA systems. LC formation is achieved only in the presence of end-to-end attraction between DNA duplexes suggesting that, similarly to bulk s-dsDNA systems, LC ordering arises from linear aggregation of DNA duplexes, even when complexed with PLL. The phase diagram of LC-coacervates can possibly be understood by principally considering only the LC ordering of s-dsDNA as a function of the DNA concentration within the coacervate dense phase. The observed phase behavior of the s-dsDNA-PLL system is more complex than that observed both for complexation of longer dsDNA,[29,30] which mainly results in precipitation, and coacervation of ssDNA, which prevalently leads to formation of unstructured liquid droplets.[17] Indeed, LC-coacervate phases were found to span the phase space between liquid coacervates and solid precipitates, while all LC mesophases could be accessed with continuity through variations of physicochemical parameters such as DNA and PLL concentration, ionic strength, and temperature.

The understanding of the structure and phase transitions of LC-coacervates, combined with robust experimental and theoretical approaches for describing phase transitions in biological LC,[31,32] can offer different insights for decoding the structure and mechanism of assembly and maturation of biomolecular condensates in cell physiology and disease.[1] The combination of coacervation and LC order also provides a framework for design of stimuli-responsive multiphase compartments[5,33] with different degrees of order in synthetic biology and drug delivery as well as for understanding how structured primitive membrane-less protocells could effect prebiotic protection, selection, and coevolution of nucleic acids and peptides.[8,9]

RESULTS AND DISCUSSION

Assembly of Liquid Crystalline Coacervates. We investigated coacervation and LC ordering in aqueous solutions of the self-complementary 12-mer DNA sequence 5′-GCGCTTAAGCGC-3′ (reverse Dickerson dodecamer (rDD)), which hybridizes into blunt-end duplexes that are known to form LCs at high concentrations (>300 mg/mL),[34,35] in combination with PLL (MW = 30 kDa−70 kDa, corresponding on average to 240 lysine (Lys) amino acids residues per chain). At a neutral pH, all DNA phosphates (P = [phosphate]) are deprotonated (pK_a of 1−2 in water),[36] contributing one negative charge from each phosphate group (*i.e.*, 11P for each rDD strand), and that all Lys ϵ-amino groups (N = [amine]) are protonated (pK_a of 10.4 in water),[37] contributing one positive charge from each Lys residue (*i.e.*, N = 240 for each PLL). The total charge concentration, Q, is thus $Q = N + P$.

Both total charge and dissolved monovalent salts play a crucial role in coacervation: a higher total charge enhances coacervation,[16] while increasing the latter weakens the interpolymer interactions by screening the electrostatic interactions,[38] often resulting in phase transitions ultimately leading to coacervate disassembly.[39] Thus, we first probed how the total charge concentration and added monovalent salts affect the structure and assembly of charge-balanced rDD-PLL mixtures (*i.e.*, $N = P$) by varying Q between 1 and 40 mM at increasing salt concentrations, up to 1 M NaCl. In Figure 1A, we report bright-field (BFTOM) and polarized (PTOM) transmitted optical microscopy micrographs at room temperature, exemplifying the observed phase behavior for a charge-balanced sample (Q = 20 mM) (Materials section). At low salt conditions, [NaCl] ≤ 700 mM, only precipitate-like birefringent structures formed (Figure 1A, purple box), while at intermediate salt conditions, 800 mM ≤ [NaCl] ≤ 900 mM, fluid coacervate droplets formed (Figure 1A, blue and magenta boxes). At higher salt conditions, [NaCl] ≥ 1M, coacervation was suppressed, and the system resulted in a uniform phase (Figure 1A, black box).

Notably at [NaCl] = 800 mM, droplets were filled by the N* LC phase (Figure 1A, blue box), as shown by the presence of typical fingerprint textures[35] in the PTOM image. These droplets were spherical (Figure S1) and fluid (Movie S1). As expected, droplets were enriched in rDD and PLL (Figure S2). Closer analysis of PTOM images revealed a right-handed chirality of the N* phase (Figure S3) with cholesteric pitch, P, >5 μm (Figure S4) within the LC-coacervate droplets. Right-handed chirality is expected when the prevailing side−side interaction between DNA helices is due to steric interactions[40] and is in accordance with the highly charge-screened conditions of our system at high salt concentrations. The cholesteric pitch of the N* phase within the LC-coacervate droplet was longer than the cholesteric pitch measured when rDD assembles into LC structures in the absence of PLL, P < 2 μm (Figure S4). An increased cholesteric pitch within the droplets indicates that PLL was relaxing the rDD helical twist and thus causing the N* macro helix to slightly unwind.

Surprisingly, we observed that a richer phase diagram could be obtained upon annealing the LC-coacervate system by heating to 90 °C followed by cooling to room temperature with a mild temperature ramp rate, $\Delta T/t \leq 5$ °C/min (Figure 1B). While annealing led to unchanged formation of N* and ISO coacervates at high [NaCl] (Figure 1B, blue and magenta boxes), the nucleation of very different phases occurred at [NaCl] ≤ 700 mM, as solid precipitates were replaced by C_U (Figure 1B, red box) and C_2 (Figure 1B, green box) LC mesophases. At 700 mM NaCl, the observation of typical "focal conic" structures (Figure 1B, red box and Figure S5), which require bending of two-dimensional hexagonally packed DNA aggregate bundles, supported the fact that the resulting phase was C_U.[21,22] At lower [NaCl], transition to the highly ordered C_2 phase was revealed by the presence of sharp-edged domains with uniform birefringence, indicating that bending of the condensed DNA was suppressed (Figure S6). In both cases, C_U and C_2 coacervates were still enriched in DNA and PLL (Figure S7).

We hypothesize that the origins of and characteristics of the LC phase arise from the supramolecular assembly of end-to-end interacting DNA duplexes within the dense coacervate phase, as it is for bulk s-dsDNA LC phases.[22,26,34] The measured intensity and direction of the local birefringence of the N* and C_U phases, $\Delta n_{N^*} = 0.018 \pm 0.001$ and $\Delta n_{Cu} = 0.034 \pm 0.001$, respectively (Figure S5), were comparable to literature values for bulk s-dsDNA LC phases,[22,41] indicating

https://dx.doi.org/10.1021/acsnano.0c05083
ACS Nano 2020, 14, 15071−15082

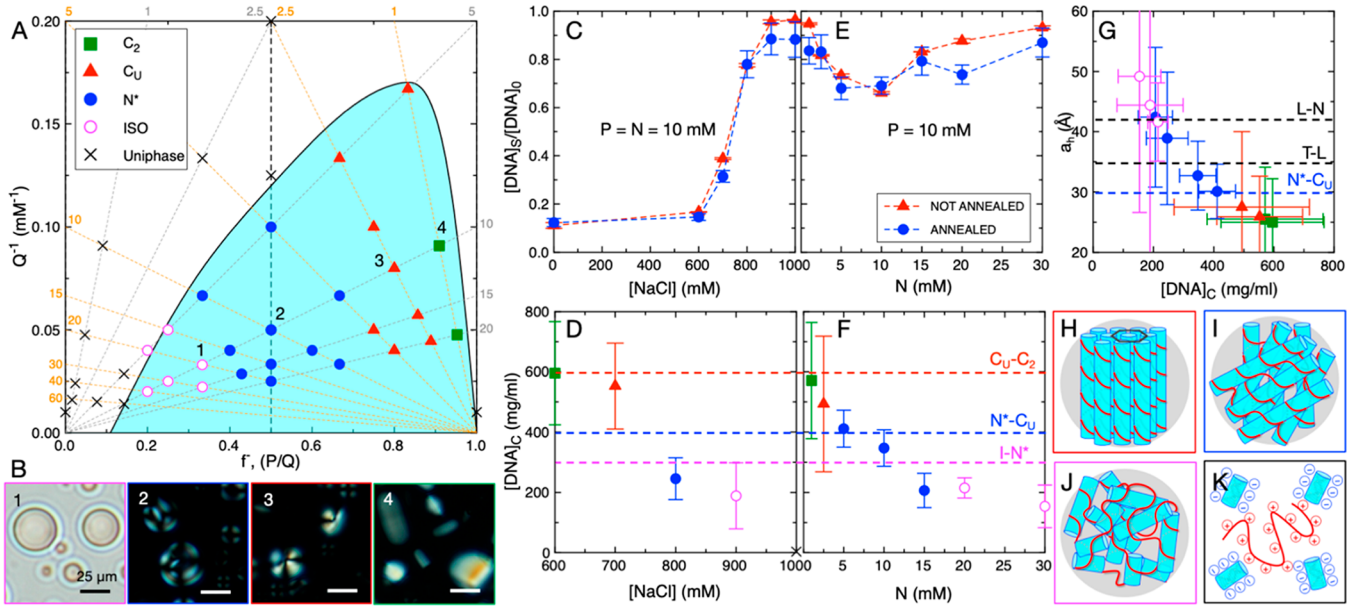

Figure 2. LC-coacervate structure. (A) Phase diagram of charge-unbalanced mixtures of non-annealed DNA-PLL. Dashed gray and orange lines: constant *P* and *N*, respectively. Cyan shading: coacervation region. Vertical dashed line: *P* = *N*. (B) Representative BFTOM images of indicated data points in (A). Scale bars are 25 μm. (C, D) Measured fraction of [DNA] in the supernatant, $[DNA]_s/[DNA]_0$ (C), and in the coacervate phase, $[DNA]_C$ (D), for rDD-PLL samples at increasing [NaCl]. (E, F) $[DNA]_s/[DNA]_0$ and $[DNA]_C$, respectively, for rDD-PLL samples at increasing N at [NaCl] = 800 mM. (C) and (E) included annealed and nonannealed samples. Horizontal colored dashed lines in (D) and (F): LC mesophase transitions for bulk rDD system.[34] (G) Calculated average interhelical distance, a_h, *vs* $[DNA]_C$ for all points from (D) and (F). Dashed lines: X-ray measured a_h at tight to lose bundles (T−L), loose bundles to isotropic network (B−L) and N*−C_U transitions.[30,48] (H−K) Possible internal conformations of coassembled s-dsDNA (teal columns) and PLL (in red) in different mesophases: (H) two-dimensional hexagonally packed tight bundles in C_U, (I) twisted nematic planes of loose bundles in N*, (J) disordered network in ISO, and (K) diluted low interacting PLL and s-dsDNA in uniform phase.

that the inner structure of the LC mesophases obtained by coacervation should not be substantially different from LC phases in bulk. Hence, the appearance of LC mesophases suggests that that even when complexed with PLL, blunt-end s-dsDNA can form reversible linear aggregates of sufficient length and stiffness, whose formation is regulated by the stacking interaction of duplex terminal base pairs. Reduced linear aggregation leads to the ISO phase.[42,43] Indeed, inhibiting the end-to-end interactions by the addition of TT overhangs at the 3′-termini of s-dsDNA duplexes causes the loss of any LC mesophase appearance and the system instead forms only unstructured ISO coacervates in a broader salt range, 200 mM ≤ [NaCl] ≤ 700 mM (Figure 1C). In the absence of end-to-end associated structures, the DNA duplex with TT overhangs is much more flexible than rDD, which assembles into rigid rod-like structures that form LC phases. It has been reported that coacervation is promoted by higher DNA flexibility,[17] even local,[18] and thus the increase in flexibility of the TT overhang-containing DNA allows this sequence to phase separate more readily under a wider range of conditions, including lower salinities. While end-to-end interaction is crucial for LC ordering to be achieved through assembly of short dsDNA (<20 bp),[22,25,26,43] similar LC ordering inside the coacervates could be achieved by sufficiently long dsDNA without such end-to-end interactions, as was observed in a previous studies in bulk DNA systems.[21] For this reason, LC coacervate mesophases could in principle be obtained in a broad range of dsDNA lengths and in the absence of end-to-end interactions under the appropriate salt, DNA, and peptide concentrations.

Since to our best knowledge, columnar DNA LC-based coacervate phases have not been reported before, it was not clear *a priori* if the phase-separated domains were liquid-like coacervates or solid-like particles. Fluorescence recovery after photobleaching[44] experiments with fluorescent PLL inside the dense phase showed that all LC mesophases analyzed, including the observed columnar mesophases, were able to recover fluorescence on the time scale of seconds to minutes, although all had slower fluorescence recovery half-times than that of ISO droplets and the uniform phase (Figure S8 and Table S1). Although this observation suggests that within LC-droplets, diffusion was slower and viscosity was higher than in the ISO phase, it confirms the fluid nature of the dense phase in all LC mesophases; this is markedly different from the solid-like behavior of precipitates. Thus, ISO, N*, and C_U coacervates could be effectively considered as fluid droplets, while the C_2 domains, predominantly characterized by nonspherical sharp-edged shapes, which relax only on longer time scales, are partially arrested glassy particles. We hypothesize that many of the undefined solid/gel-like particles observed in similar coacervate systems[17,18] could have been instead columnar LC phases which had not been recognized at the time of these studies. Re-examination of such systems with more complex visualization techniques, such as polarized optical microscopy, X-ray scattering, or transmission electron cryomicroscopy (which was performed in similar systems[45]), combined with a larger survey of environmental conditions (salt, DNA and peptide concentrations), could indeed reveal the presence of LC phases.

Charge-Unbalanced DNA-PLL Mixtures. To understand the structural role of PLL within the LC-coacervate

https://dx.doi.org/10.1021/acsnano.0c05083
ACS Nano 2020, 14, 15071−15082

mesophases, we studied the phase behavior of charge-unbalanced rDD-PLL mixtures, i.e., $P \neq N$, (Figure 2A,B) by varying the total final concentration of positive and negative charges in the range of 1 mM < P < 20 mM (dashed gray lines, Figure 2A) and 1 mM < N < 60 mM (dashed orange lines, Figure 2A), while maintaining a constant [NaCl] = 800 mM. The data are plotted as a function of the fraction of negative charges, $f^- = P/Q$, and of the inverse of the total charge, Q^{-1}. The former parameter is a measure of the DNA-PLL ratio: if $f^- > 0.5$, then the system is richer in DNA and *vice versa*. The latter is a measure of the strength of the electrostatic interactions which drive coacervation: at high Q (*i.e.*, low Q^{-1}), coacervation is enhanced, and *vice versa*.[16] At low DNA concentrations, P < 5 mM, the system remains in the uniform phase, independent of PLL concentration (black crosses). At $P \geq 5$ mM, coacervation starts to occur (cyan shaded region, Figure 2A), leading to the formation of C_U (red triangles, Figure 2A), N* (blue dots, Figure 2A), and ISO phases (magenta open dots, Figure 2A) with increasing N. At high N, that is, $f^- < 0.2$, coacervation is again suppressed. The general trend appears to be that at increasing P, the different phase transitions take place at increasing N (Figure S9). Moreover, at low N, the formation of the C_2 phase is observed only for $P \geq$ 10 mM (green squares, Figure 2A).

Contrary to the charge-balanced mixtures reported above, here the C_U and C_2 phases appear even without annealing. We attribute this phenomenon to two reasons, both related to the potential ability of the peptide and DNA to rearrange in order to escape precipitation. First, the NaCl concentration used was 800 mM. At this sufficiently high salt concentration, we did not observe precipitates forming under any conditions, suggesting that weaker DNA-PLL complexation could facilitate the system to escape the energetically trapped precipitate state and to assembly into the columnar LC state. Second, at $N \ll P$ (where the columnar phases were observed), the DNA-PLL charge unbalance is reflected also in the composition of the dense coacervate phase:[46,47] there is an excess of DNA over PLL that could facilitate the rearrangement of peptide-DNA bridging, in turn providing a much more fluid environment that finally allows the columnar ordering to prevail over precipitation.

All of these observations also suggest that, while PLL presence is essential for phase separation through coacervation, it can also interfere with DNA packing in the LC phases: the phases with higher degrees of order, that is, C_U and C_2, arise only at low PLL content, $N \ll P$, while transition to unstructured isotropic coacervates takes place at greater prevalence of PLL, $N \gg P$, where DNA duplexes are arguably diluted by the excess of flexible cationic polymers.

Phase Dependence on Concentration/Salt and LC-Coacervate Assembly Mechanism. The observations reported above show that similar phase behavior could be achieved both by variations of salt concentration in charge-balanced mixtures and by variations in N/P ratio in charge-unbalanced mixtures at constant [NaCl]. This suggests that a single parameter which is dependent on both [NaCl] and N/P could, in fact, be the main driver of phase behavior. We propose this parameter to be the concentration of DNA in the dense coacervate phase, $[DNA]_C$, as both [NaCl] and N/P affect $[DNA]_C$ during complex coacervation,[47] while the phase behavior of a lyotropic LC system also principally depends on the concentration of the molecular species responsible for the LC ordering.[20,22,34]

We first indirectly estimated $[DNA]_C$ by measuring the concentration of DNA in the supernatant, $[DNA]_S$, and the volume fraction of the dense phase, Φ_C, at P = 10 and varying [NaCl] and N (Figures 2C–F and S10 and Supplementary Note SN1). The fraction of DNA in the supernatant, $[DNA]_S/[DNA]_0$, provides additional information about the degree of rDD-PLL complexation, and therefore an indicator of coacervation efficiency.[10,17] We observed that indeed the supernatant was depleted of DNA at low [NaCl] (≤600 mM), conditions in which there is strong DNA-PLL complexation, while increasing [NaCl] above 600 mM results in an increase in $[DNA]_S/[DNA]_0$ due to higher screening of the electrostatic interactions between rDD and PLL favoring dissociation (Figure 2C). Such behavior is independent of annealing, suggesting that the transition between precipitates and LC columnar phases is mostly related to the reorganization of the polymers inside the dense phase. The formation of ISO and N* coacervates involves only 10%–20% of the total DNA in the dense phase, suggesting that ISO and N* mesophase formation takes place in a regime of low rDD-PLL coacervation efficiency. The same feature was also observed in unbalanced charge mixtures, where maximum coacervation efficiency was achieved around charge neutrality, $N = P$ (Figure 2E). However, for C_2 and C_U phases emerging at low N, high values of $[DNA]_S/[DNA]_0$ were observed: the high supernatant DNA concentration is likely a direct effect of the overall low PLL content in these samples, which results in less total DNA able to exist in a condensed state due to a lack of a binding partner polycation (PLL).[46,47]

Despite the uncertainties in the measurement of Φ_C, $[DNA]_C$ can provide important information for the understanding of the assembly mechanism of LC coacervates in different mesophase regimes. $[DNA]_C$ was found to vary from 150 mg/mL, for the low-density ISO phase, to 600 mg/mL, for the highly ordered columnar phases (Figure 2D,F); this range of [DNA] is typical for the onset of LC ordering in bulk s-dsDNA systems.[22,25,26,34] In particular, DNA concentrations of LC mesophases in the coacervates are compatible with the rough phase boundaries (dashed lines in Figure 2D,F) reported for LC ordering in bulk solutions of a comparable DNA 12-mer molecule.[34]

This fact indicates that, by first approximation, the phase diagram of PLL-induced LC-coacervates can possibly be understood by principally considering only the LC ordering of s-dsDNA as a function of $[DNA]_C$. An increase in $[DNA]_C$ results in an increase of the average length of s-dsDNA aggregates, which drives the ISO to LC transition as reported in theoretical models for linear reversible aggregation.[42] The presence of PLL could also contribute to increasing the local concentration of DNA inside the dense phase, especially for the charge-unbalanced mixtures at high N, thus enhancing the compatibility of the phase boundaries with that of the pure DNA system (Figure 2F).

Knowing $[DNA]_C$ also allows the calculation of the average interhelical distance, a_h, by considering DNA aggregates hexagonally packed (Supplementary Note SN2). The obtained values of the interhelical distance, a_h, calculated from $[DNA]_C$, are in the range 25–30 Å for C_2 and C_U, 30–40 Å for N*, and a_h > 40 Å for ISO (Figure 2G). Even if subjected to large uncertainties, these values provide rough information on the internal structure and on the degree of long-range ordering of rDD-PLL LC coacervates, which complement the macroscopic information obtained by PTOM textures and birefringence

https://dx.doi.org/10.1021/acsnano.0c05083
ACS Nano 2020, 14, 15071–15082

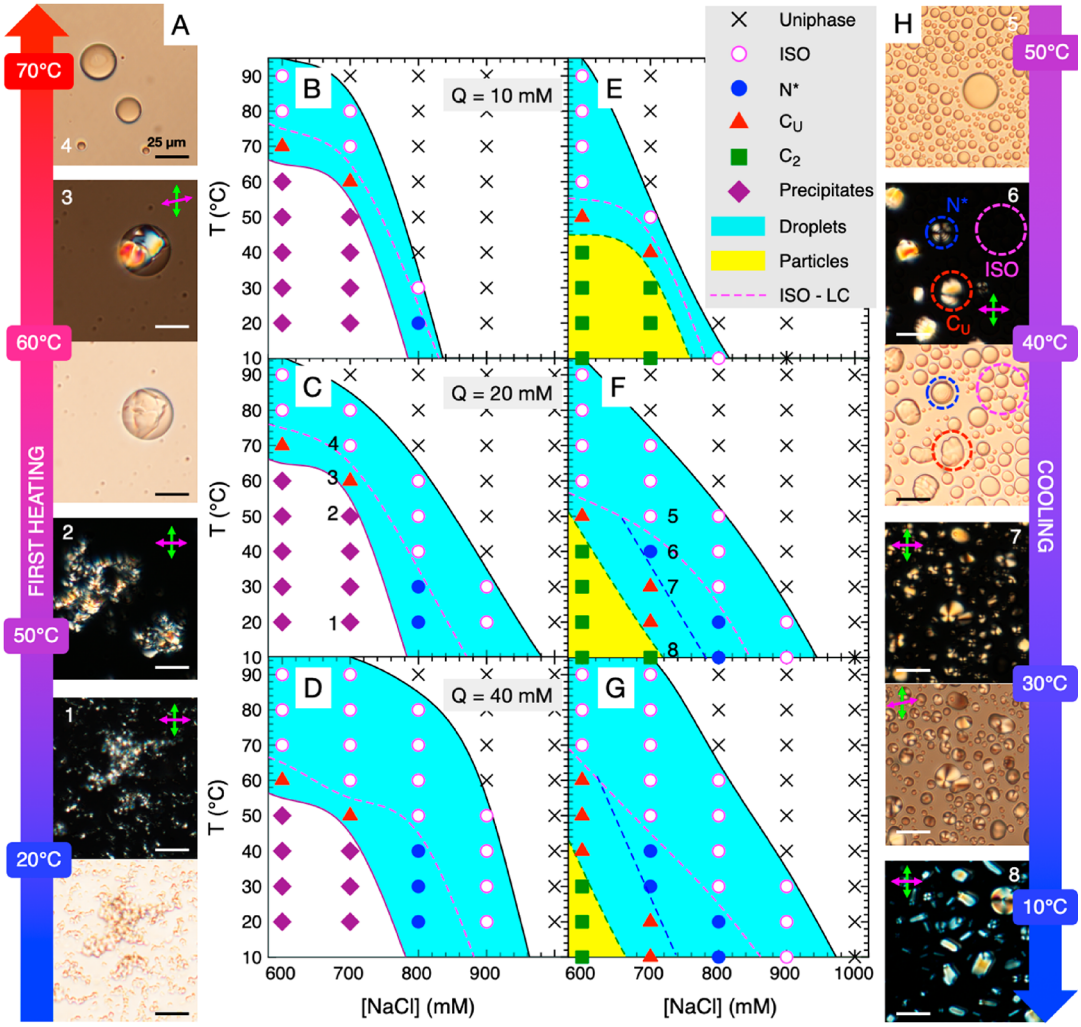

Figure 3. Thermal stability and annealing of LC-coacervates. (A) Representative BFTOM and PTOM images of an rDD-PLL mixture (Q = 20 mM, [NaCl] = 700 mM). Precipitates (1) rearrange (2) and are replaced by C_U-ISO (3) and ISO (4) coacervates upon heating. (B–D) [NaCl]-T phase diagrams of rDD-PLL mixtures at Q = 10 mM (B), 20 mM (C) and 40 mM (D) during the first heating of the systems. Images in (A) represent the indicated points in (C). (E–H) [NaCl]-T phase diagrams obtained upon cooling of the same samples in (B–D), respectively, and representative BFTOM and PTOM images (H) corresponding to the indicated points in (F). At high temperature, ISO coacervates form (5) and subsequently simultaneously nucleate C_U and N* (coexisting with ISO) upon cooling depending on [NaCl] (6). Further cooling transitions the systems to C_U (7) and C_2 (8) (but not precipitates) at low [NaCl]. Cyan region: region of fluid coacervate formation. Solid purple line: precipitate boundary. Solid black line: uniform phase boundary. Dashed lines: ISO-N* (magenta), N*-C_U (blue), and C_U-C_2 (green) transitions in coacervates, always involving coexistence. Lines, generated by visual inspection, do not represent data. Yellow region: transition from fluid droplets to particles takes place at the insurgence of C_2.

measurements. These observations together suggest that the C_U phase can be characterized by tight hexagonal packing of DNA-PLL bundles (Figure 2H), which becomes longitudinally locked in the C_2 phase. The loosening of the bundles allows the onset of the N* phase, in which nematic planes have enough freedom to twist and form the characteristic cholesteric macro-helical super structure (Figure 2I). The ISO phase is then characterized by a disordered fluid of shorter DNA aggregates randomly bridged by flexible PLL polymers (Figure 2J), which is the typical conformation of liquid dsDNA based coacervates.[17] Finally, coacervate disruption and a diluted uniform phase are the result of weak DNA-PLL complexation (Figure 2K). Transitioning from C_2 to the uniform phase (*via* C_U, N*, and ISO), both the DNA-PLL interaction strength and supramolecular aggregation decrease, affecting the degree of order of the system as shown in Figure 2H–K.

The observed phase behavior and the resulting proposed LC coacervate structures (Figure 2) are in agreement with the reported observations that variations in the internal spacings of DNA-polycation complexes are dependent on salt concentration[30,48] and on charge unbalance.[46,47] Indeed, X-ray scattering experiments have shown that PLL-induced calf-thymus DNA complexes are hexagonally packed and can undergo discontinuous phase transitions from tight bundles to lose bundles and finally to an isotropic network phase at increasing monovalent salt concentrations,[30] with interhelical spacings compatible with our observations (dashed black lines in Figure 2G). Moreover, long dsDNA-spermine complexes have been shown to produce liquid crystalline precipitates which are either C_U or N*, with ionic strength-dependent interhelical spacing varying between 28.15 and 33.4 Å, and a C_U-N* discontinuous transition at $a_h \approx 30$ Å[48] (dashed blue

https://dx.doi.org/10.1021/acsnano.0c05083
ACS Nano 2020, 14, 15071–15082

line in Figure 2G), which is roughly in agreement with our observations of the rDD-PLL LC system in this study.

Finally, DNA-PLL LC coacervation and transitions between mesophases could be triggered by cooperative DNA-PLL binding, similar in principle to what has been reported for DNA plasmid condensation with PLL.[49] At high [NaCl], PLL cooperatively interacts with DNA, that is, the initial binding of PLL to an individual DNA molecule forming a nucleus of condensation is followed by subsequent PLL binding at neighboring sites, while at low [NaCl], noncooperative binding is favored, inducing random PLL cross-linking. This is further supported by molecular dynamics simulations of the binding between a comparable dsDNA 12-mer and short PLL, suggesting that in a hexagonally packed DNA-PLL condensed phase, the interhelix distance of 30 Å is achievable only if there is one PLL chain bridging between the two DNA helixes.[50]

Thermal Stability and Annealing of LC-Coacervates. Since the thermal annealing process was shown to be crucial for the solid precipitate structures to be replaced by columnar LC mesophases (Figure 1), we further characterized the mesophase transitions of the LC-coacervate system as a function of temperature, T, between 10 and 90 °C. We monitored rDD-PLL charge-balanced mixtures, at different total charges, $10 \leq Q \leq 40$ mM, and varying [NaCl], 600 mM $\leq$ [NaCl] $\leq$ 1 M, while gradually increasing the temperature (Figure 3A−D). The general trend observed while increasing T appears to be the rearrangement of the birefringent precipitate structures (Figure 3A, images 1 and 2), whose domains gradually achieve smoother shapes of phase-separated droplets displaying columnar textures (Figure 3A, image 3). Subsequent melting into ISO coacervates was observed at further heating (Figure 3A, image 4). In all cases, LC phases melt into the ISO phase *via* a first-order transition characterized by a temperature range of phase coexistence inside the coacervate droplets, as usually observed in bulk s-dsDNA LC systems.[22,25,26] Finally, the ISO droplets disappear at higher T, where the system preferentially resides in a uniform phase (Figure 3B−D), indicating that thermal agitation has overcome the strength of the electrostatic interaction between DNA and PLL, leading to coacervate disassembly. The thermal stability of the coacervate droplets appears to decrease at increasing [NaCl] due to the weakening of polyelectrolyte complexation due to screening of electrostatic charges.[38] For example, at higher [NaCl], the ISO phase melts and transitions to a uniform phase at a lower temperature than at lower [NaCl]. Similarly, the LC to ISO transition occurs at a lower temperature at increasing [NaCl] (magenta dashed lines).

The permanence of LC phases at fairly high temperatures (*e.g.*, 70 °C at 600 mM NaCl) provides additional information on the hybridization state and the end-to-end interactions of DNA. Indeed, since s-dsDNA LC formation requires long, stiff molecular aggregates,[42] these should be present whenever LC is observed.[22] Moreover, the existence of a LC-coacervate phase is predicted only at sufficient polyanion rigidity.[28] The observation of bulk s-dsDNA LC phases at high temperatures and experimental verification of DNA hybridization under such conditions has been reported in previous works[24,25,51] through monitoring the fluorescence emission of intercalating ethidium bromide molecules. LC phase and duplex DNA existence at high temperatures is a direct consequence of the fact that the high DNA concentration achieved in the LC phase, which in this case is enhanced within the dense coacervate phase (Figures 2D−F), leads to an increase in duplex melting temperature, T_m (as DNA melting depends on strand concentration).[52] It has been reported that DNA 12-mers can reach $T_m \approx 60-70$ °C at [DNA] $\approx$ 600−800 mg/mL[24] (*i.e.*, the same range as the system studied herein), while DNA as short as tetramers, which normally do not hybridize at room temperature, can reach a $T_m \approx 50$ °C at [DNA] $\approx$ 100 mg/mL.[51] Further increases in temperature result in the appearance of the ISO coacervate phase, which likely includes non-end-to-end aggregated dsDNA and/or dehybridized ssDNA.

We then further characterized the temperature-induced structural transitions of LC-coacervates by cooling heated systems at various Q and [NaCl] (Figure 3E−H); the cooling was performed at the same rate as heating. Eventually starting from a uniform phase at high T, the ISO coacervate phase forms following a nucleation and growth process upon cooling (Figure 3H, image 5). ISO phase emergence is dependent on salt concentration, with the ISO phase re-emerging at lower temperatures at higher [NaCl] due to weaker polyelectrolytes complexation, similar to that observed during heating Figure 3A−D. Upon further decreasing T, C_U or N* nucleation inside the coacervates eventually occurs, leading first to phase coexistence (Figure 3H, image 6) and then to the formation of fully LC droplets at different [NaCl] (Figure 3H, image 7). At lower [NaCl] and lower Q, a C_U-C_2 transition was observed upon further cooling (Figure 3H, image 8), resulting in a large decrease of the fluidity in the phase-separated domains attributed to a transition from droplets to glassy particles (cyan shading to yellow shading in Figure 3E−G). In general, the temperature at which each transition occurred, as well as the total region where coacervation is allowed, during both heating and cooling increased with increasing Q values, as higher temperatures are needed to disrupt the stronger intermolecular interactions at high Q[16] (Figure 3B−D,E−G).

Precipitate formation was not observed by further cooling the annealed systems even below the initial preparation temperature, T = 20 °C, as the LC phase persisted. This indicates that, depending on [NaCl], LC or ISO coacervates are likely to be the phases with the most stable conformation and constitute the global ground state of the system. It is likely that the precipitates that were formed upon initial mixing of the components at room temperature exist only as local minima of the energy landscape (similar to a kinetic trap) achieved during the sudden and disordered complexation of rDD and PLL. We posit that the initial rDD-PLL complexation at room temperature causes the formation of highly concentrated regions where the DNA is hexagonally packed, thus giving a birefringent signal in PTOM images. However, the sudden nucleation of columnar seeds is not followed by sufficient growth time for the C_U domains, resulting instead in precipitate formation. Instead, when the system is slowly cooled from high T, the nucleation and growth process may have sufficient time to occur. Moreover, in this case the entire self-assembly could benefit from rearrangement of DNA-PLL binding at high T, eventually enhancing cooperative binding of the two polymers[49] and settling on more stable conformations, which could include diminishing intercolumnar cross-linking.[30] This process, energetically, would be similar to the annealing process (through cooling) crucial for the formation of DNA origami structures in DNA nanotechnology applications.[53]

Continuity of the LC-Coacervate Mesophases. One additional observation gleaned from the phase diagrams in Figure 3 is that the dense coacervate phase appears to be able

https://dx.doi.org/10.1021/acsnano.0c05083
ACS Nano 2020, 14, 15071−15082

to access the different LC mesophases with continuity as a function of all of the tested physical variables which govern the assembly of the system: temperature, monovalent salt concentration, and total charge, with the latter being dependent on the molar concentration of rDD and PLL. The direct consequence of this observation is that upon evaporation and rehydration, the system could potentially explore all achievable states set by its initial preparation in continuous fashion. For example, a sample prepared at $N = P =$ 5 mM and [NaCl] = 700 mM, which initially formed only precipitates (Figure 4A), will undergo subsequent transitions to C_U and N* LC phases (Figure 4B–C) upon drying. Such phase transitions are driven by the gradual increase of Q and [NaCl], the latter causing larger screening of the electrostatic interactions which promote the swelling of the coacervates and also their final transition to ISO droplets[30] (Figure 4D). Ultimately, complete disassembly and transition to a uniform phase (Figure 4E) are achieved at sufficiently high [NaCl] caused by water loss (see Movie S2). This behavior is similar to what has been reported for aqueous solutions of stoichiometric polyelectrolyte complexes, which can span the continuity of possible structural space, from solid complexes, to liquid droplets, to the uniform phase, by tuning the concentration of KBr (potassium bromide).[39]

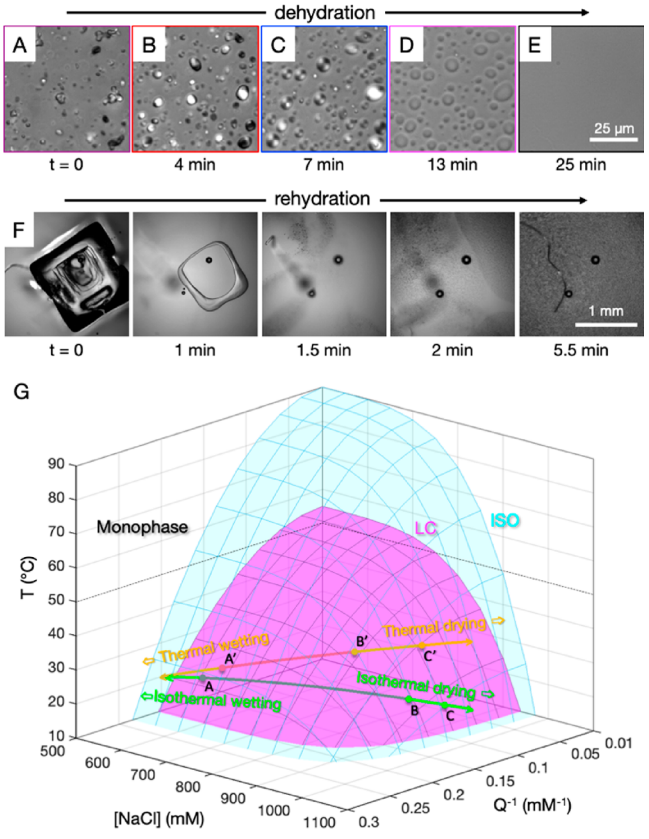

Figure 4. Continuity of the coacervate LC mesophase transitions. (A–E) partially crossed PTOM images of rDD-PLL sample ($N = P$ = 5 mM, [NaCl] = 700 mM) during dehydration at room temperature over several minutes, causing continuous transitions from precipitate (A), to C_U (B), to N* droplets (C), to ISO droplets (D), to a uniform phase (E). (F) Complete drying results in macroscopic salt crystal formation, which is melted by subsequent rehydration, causing the re-emergence of LC-coacervation over time. (G) 3D plot of phase diagram of LC coacervates as a function of T, [NaCl], and Q^{-1}, built from plots in Figures 3E–G. Cyan surface: region of parameter space where coacervation is allowed. Magenta surface: region of LC formation (entirely within cyan surface). At moderate temperatures, 0 °C < T < 50 °C, LC mesophases are more common than the ISO phase in coacervate droplets. Isothermal drying-wetting cycles correspond to equilateral hyperboles on the [NaCl]-Q^{-1} plane (green line), which intersects all phase boundaries (1, 2, and 3: intersection points with phase boundary surfaces). Temperature variations during drying–wetting cycles, for example, drying at increasing T and wetting at decreasing T, result in vertical span (orange line), but can still intersect all phase boundaries (1′, 2′, and 3′: intersection points with phase boundary surfaces).

This observation suggests that the LC-coacervate system can escape from precipitation by drying, which is exactly contrary to what typically occurs in dsDNA solutions, where drying precipitates would likely only result in either more precipitates or at least persistence of the initial precipitates. The reverse process can also occur upon water addition to high-concentration uniform phase systems or even to fully dried samples. For example, rehydration of a fully dried sample displaying only macroscopic [NaCl] crystals (Figure 4F) results in a gradual decrease of [NaCl], which drives the formation of condensed coacervate phases and can ultimately lead back to the initial precipitate state (Figure 4F and Movie S3).

One feature of the system studied herein is the fact that the LC-coacervate mesophases are located at intermediate concentrations of tested salt and analytes, which suggests that upon repeated drying-wetting cycles (or simply changes in salinity), these phases could in principle be repeatedly accessed even upon reaching either end of the phase scale (Figure 4G, green line). Moreover, since phase transitions between system states can also be simultaneously performed as a function of temperature, all LC mesophases can be reliably accessed in a continuous fashion by combining dehydration–rehydration processes with temperature variations (Figure 4G, orange line). The LC phases are more common than the ISO phase in coacervate droplets at moderate temperature, T < 50 °C, and exhibit the most peculiar properties because of their ordered but still fluid nature, which could overcome structural and functional limitations of both unstructured diluted liquids and completely static precipitates.

CONCLUSIONS

We have shown that LC phases can be assembled in conjunction with coacervate droplets composed of a cationic peptide and s-dsDNA. Surprisingly, we found that in addition to classical liquid coacervates, in a regime in which solid precipitate or gel-like particles were usually observed,[17,18] the complete set of known LC mesophases (N*, C_U, and C_2) typical of the bulk hierarchical self-assembly of s-dsDNA are instead accessible continuously (Figures 1 and 2). The formation of these LC-coacervate mesophases can be controlled completely through variations in PLL and DNA concentration, [NaCl], and temperature (Figures 2 and 3). Additionally, the LC-coacervate phases still remain fluid, and the entire assembly is dynamic and reversible. The supramolecular structure of the entire coassembly can also be described using the same approach describing LC formation in bulk,[22,26,34,42] with the addition of DNA-PLL complexation.[30,49] Surprisingly and contrary to the behavior of single component solutions, both the drying of solid precipitate states

https://dx.doi.org/10.1021/acsnano.0c05083
ACS Nano 2020, 14, 15071–15082

and the dilution of a uniform liquid phase induce the emergence of ordered phases (Figure 4).

Both LC ordering of short nucleic acids[22−26] and coacervation induced by cationic peptides,[10,17,54] separately, have been shown to be robust phenomena whose assembly and properties are dependent on polymer length, sequence, and structure. For this reason, it is plausible that, due to being a combination of short nucleic acids and cationic peptides, LC-coacervate assemblies could also be generally achieved in a broad range of nucleic acid/peptide combinations and concentrations under the proper conditions. The propensity of LCs to segregate DNA molecules by flexibility[55] or by structure[24] could also provide an effective mechanism to generate multiphase coacervate droplets, without the need of mixing numerous different species of polyelectrolytes.[33] The resulting different internal phases would differ not only in density but also in their degree of order, thus having radically different permeabilities to and preferences for eventual guest molecules depending on their physicochemical properties. For example, stiff linear polymers[55] or small flat aromatic molecules[56] could be hosted in a LC phase within a droplet, while flexible globular polymers, such as enzymes or ribozymes, could be segregated within a ISO phase within the same droplet.[55] Such features could be relevant for tuning biochemical reactions[57] or for improving stimuli response[58] in coacervate systems with applications in bottom-up synthetic biology.[5,6]

In the context of prebiotic chemistry, membraneless coacervate microdroplets have been proposed to be a relevant model of primitive compartment systems,[9,10,54] while LC phases have been shown to provide a templating environment capable of catalyzing prebiotically relevant chemical reactions such as nonenzymatic nucleic acid ligation.[59,60] The combination of these two self-assembly mechanisms could provide an additional pathway by which prebiotic systems increased in structural and functional complexity. This and other studies have shown that coacervation can increase the local concentration of analytes by many orders-of-magnitude.[10,15] Given the fact that the required DNA concentration for LC assembly in bulk is fairly high (∼10−1000 mg/mL)[22,25,26] and unlikely to have been available on prebiotic earth, coacervation of duplex nucleic acids could be the preferential mechanism by which primitive LC phases could be accessed. Additionally, LC ordering has also been shown to take place in pools of both random nucleotides[26] and random sequence nucleic acid oligomers,[24] the latter being the most probable outcome of any abiotic nucleic acids polymerization process.[61] Coacervation can be induced by a variety of oligomers of prebiotic relevance,[54] perhaps also in a random fashion. In the presence of the proper activation chemistry[62] within a mixed random peptide-nucleic acid system, both species could feasibly continue polymerization and explore the sequence space sustained by cooperative peptide-nucleic acid binding,[49] which could foster the coevolution of the co-assembled polymers. In this frame, the onset of LC ordering could have potentially enhanced the elongation of linear complementary nucleic acids by ligation,[59,60] eventually selected folding (potentially active) sequences by selective partitioning[55] and provided a template for peptide polymerization.[62] LC-coacervation could also have been one mechanism by which a primitive system increased its structural complexity and resistance to dissolution: by phase transitions in response to environmental changes such as temperature and hydration variations achieved through diurnal or seasonal drying-wetting and thermal cycles in coastal oceanic or inland environments.[63,64]

Lastly, LCs are strongly connected to biology and biochemistry. On the one hand, LC ordering has been observed in *in vitro* solutions of several different biomolecules, including nucleic acids, proteins, and lipids,[32] and on the other hand, *in vivo* LC ordering is known to play a major role in dsDNA compaction in prokaryotic cells and in favoring DNA repair after damage.[29] During the past decade, typical concepts in LC theory, such as nematic ordering and topological defects, have been applied to describe apparently unconnected systems, for example, active biological systems with different degrees of order, such as cytoskeleton biopolymers, and bacterial suspensions, which have been named active nematics,[65] or even proposed for modeling the microtubule spindle in the process of mitotic cell division.[66] In this view, LC-coacervates composed of dsDNA and cationic peptides, while not yet observed *in vivo*, could be exploited as a model system to gain insight into the structural properties and phase transitions in the assembly and maturation of membraneless organelles in living cells, often associated with diseases.[1] Further exploration of additional variables driving LC-coacervate assembly, such as component length, sequence, structure, charge, hydrophilicity, and flexibility, may result in a deeper understanding of the fundamental parameters governing the phase diagram of biological phase-separated systems.

METHODS

Materials. All chemicals were purchased from Sigma-Aldrich, Inc. (St. Louis, Missouri, USA) unless otherwise indicated, including PLL (poly-L-lysine hydrobromide 30−70 kDa, P2636) and PLL-FITC (fluorescein isothiocyanate-labeled poly-L-lysine 30−70 kDa, P3069). DNA rDD (5′-GCGCTTAAGCGC-3′) was synthesized with an Akta-Oligopilot (GE Healthcare Life Sciences, Marlborough, Massachusetts, USA) and purified by HPLC (Varian Prostar 218 system, Varian, Palo Alto, California, USA) as described elsewhere.[24] rDD was dialyzed against 1 L of 10 mM NaCl for 48 h, replacing the dialysis buffer after 2, 4, and 12 h and subsequently lyophilized. DD-TT (5′-CGCGAATTCGCGTT-3′) and DD-TAMRA (5′-TAMRA-CGCGAATTCGCG-3′; TAMRA is carboxytetramethylrhodamine) HPLC grade were purchased from Primm S.r.l. (Milano, Italy) and from Integrated DNA Technologies (Coralville, Iowa, USA), respectively, and used without further purification. All solutions were made in Milli-Q water, Millipore (Burlington, Massachusetts, USA).

Sample Preparation. Stock solutions of rDD and PLL of 100 mM total charge (negative charges from the rDD phosphate groups (P) and positive charges from the PLL amino groups (N)), as well as a 4 M stock solution of NaCl, were prepared. From these stock solutions, 10 μL solutions of rDD, PLL, and NaCl were produced in a plastic 0.2 mL microcentrifuge tube (Eppendorf, Hamburg, Germany) to obtain the desired analyte concentrations, as indicated in the relevant text and figures. It is important to note that NaCl should be added to the solution before mixture of rDD and PLL to avoid precipitation. Samples were prepared by adding salt, then PLL, then DNA, always following this addition sequence, even if no difference was found in adding DNA before PLL. The solution pH was around 7.0, and no buffer was added to regulate pH. All solutions were prepared at room temperature.

Microscopy Analysis. Initially, each glass microplate was passivated by adding a 3.5% bovine serum albumin solution to each well for 15 min at room temperature, then rinsed with nuclease-free water, and dried. Passivation is used to avoid droplet coalescence once deposited on the bottom surface. All the experiments were also prepared without glass passivation, as passivation was not found to

https://dx.doi.org/10.1021/acsnano.0c05083
ACS Nano 2020, 14, 15071−15082

affect the phase behavior. We deposited 10 μL of each prepared rDD-PLL solution to the bottom of a 96/384 well glass microplate (Corning, New York, New York, USA). To that, 40 μL of "light" mineral oil (M5904, Sigma-Aldrich) was added to the top of each sample, followed by application of a plastic PCR film (Biorad, Segrate, Italy) to prevent evaporation (in some experiments involving evaporation or rehydration, this step was omitted). Optical and polarization microscopy images of each sample were acquired with a Nikon (Shinagawa-ku, Tokyo, Japan) Ti–U inverted fluorescent microscope equipped with linear polarizer and analyzer, whose orientations are indicated in each image, if relevant. All samples were observed at room temperature unless otherwise indicated. Temperature was controlled with a TSA12 Gi Peltier hot/cold stage (Instec, Colorado, USA). Observation was undertaken after at least 10 min incubation time, to allow each phase to reach equilibrium. The sign and magnitude of the birefringence in textures were determined by use of variable compensators, Berek type (Nichika Corporation, Kyoto, Kyoto, Japan), on a Nikon Eclipse Ni-E optical microscope.

For samples involving fluorescence observations, including Z-stacking, fluorescently PLL-FITC or DD-TAMRA was added to unlabeled solutions at a 1:1000 ratio. Fluorescence microscope images were acquired with a Leica (Wetzlar, Germany) SP8 confocal fluorescence microscope using a 20× objective (NA: 0.75) with blue (405 nm) or green (488 nm) laser excitation (Diode Laser) with the appropriate emission channels. Heated samples utilized a Tokai Hit (Fujinomiya, Shizuoka, Japan) stage top heating system. All images were analyzed using FIJI (Fiji is Just ImageJ, http://fiji.sc). Observations were performed in at least duplicate.

ASSOCIATED CONTENT

Supporting Information

Supporting information and movies can be found in the Supporting Information available online. The Supporting Information is available free of charge at https://pubs.acs.org/doi/10.1021/acsnano.0c05083.

Supporting figures, discussion, and detailed description of some data analysis (PDF)

Movie S1: Coalescence of cholesteric, N*, rDD-PLL LC-coacervate droplets at $N = P = 10$ mM and 800 mM NaCl (AVI)

Movie S2: Drying of 5 μL solution of an rDD-PLL LC-coacervate system ($N = P = 5$ mM and 700 mM NaCl) over time (AVI)

Movie S3: Reformation of LC-coacervates upon rehydration of a dried rDD-PLL LC-coacervate system ($N = P = 5$ mM and 700 mM NaCl) (AVI)

AUTHOR INFORMATION

Corresponding Author

Tommaso P. Fraccia − *Institut Pierre-Gilles de Gennes, Chimie Biologie Innovation, ESPCI Paris, CNRS, PSL Research University, 75005 Paris, France;* orcid.org/0000-0002-9638-4269; Email: tommaso.fraccia@espci.fr

Author

Tony Z. Jia − *Earth-Life Science Institute, Tokyo Institute of Technology, Tokyo 152-8550, Japan; Blue Marble Space Institute of Science, Seattle, Washington 98154, United States;* orcid.org/0000-0001-5175-4599

Complete contact information is available at: https://pubs.acs.org/10.1021/acsnano.0c05083

Author Contributions

‖These authors contributed equally. Both authors designed and performed experiments, performed data analysis and wrote the manuscript.

Notes

The authors declare no competing financial interest.

ACKNOWLEDGMENTS

We would like to thank D. Cuvelier, T. Lopez-Leon, and Y. Kuruma for the use of their microscopes during parts of this study and B. Cinquin, engineer at the IPGG platform, for support with confocal measurements. We are indebted to T. Bellini, N. A. Clark, A. Griffiths, A. Soranno, and A. Wang for critical reading of the manuscript and useful discussions. T.P.F. is supported by an IPGG Junior Research Chair fellowship and from the IPGG Équipement d'Excellence grant, "Investissements d'avenir," program ANR-10-EQPX-34. T.Z.J. is a researcher at the Earth-Life Science Institute (ELSI) at Tokyo Institute of Technology, which is supported under the World Premier International Research Center Initiative of the Japan Ministry of Education, Culture, Sports, Science, and Technology, and is further supported by JSPS Kakenhi Grant-in-Aid JP18K14354, Japan Astrobiology Center (National Institutes of Natural Sciences (NINS)) Project grants AB311021 and AB021008, Tokyo Institute of Technology Seed Grant "Tane" 1798, and a Programme Exploration France travel grant from the French Embassy in Japan. Initial discussions and experiments were supported by travel funding from the ELSI research interactions committee and a seed grant from the ELSI Origins Network (EON) which was supported by a grant from the John Templeton Foundation. The opinions expressed in this publication are those of the authors and do not necessarily reflect the views of the John Templeton Foundation.

REFERENCES

(1) Shin, Y.; Brangwynne, C. P. Liquid Phase Condensation in Cell Physiology and Disease. *Science* **2017**, *357*, No. eaaf4382.
(2) Yoshizawa, T.; Nozawa, R. S.; Jia, T. Z.; Saio, T.; Mori, E. Biological Phase Separation: Cell Biology Meets Biophysics. *Biophys. Rev.* **2020**, *12*, 519–539.
(3) Alberti, S.; Dormann, D. Liquid–Liquid Phase Separation in Disease. *Annu. Rev. Genet.* **2019**, *53*, 171–194.
(4) McSwiggen, D. T.; Mir, M.; Darzacq, X.; Tjian, R. Evaluating Phase Separation in Live Cells: Diagnosis, Caveats, and Functional Consequences. *Genes Dev.* **2019**, *33*, 1619–1634.
(5) Martin, N. Dynamic Synthetic Cells Based on Liquid − Liquid Phase Separation. *ChemBioChem* **2019**, *20*, 2553–2568.
(6) Schwille, P.; Spatz, J.; Landfester, K.; Bodenschatz, E.; Herminghaus, S.; Sourjik, V.; Erb, T. J.; Bastiaens, P.; Lipowsky, R.; Hyman, A.; Dabrock, P.; Baret, J.-C.; Vidavich-Koch, T.; Bieling, P.; Dimova, R.; Mutschler, H.; Robinson, T.; Tang, T.-Y. D.; Wegner, S.; Sundmacher, K. MaxSynBio: Avenues towards Creating Cells from the Bottom Up. *Angew. Chem., Int. Ed.* **2018**, *57*, 13382–13392.
(7) Indulkar, A. S.; Gao, Y.; Raina, S. A.; Zhang, G. G. Z.; Taylor, L. S. Exploiting the Phenomenon of Liquid-Liquid Phase Separation for Enhanced and Sustained Membrane Transport of a Poorly Water-Soluble Drug. *Mol. Pharmaceutics* **2016**, *13*, 2059–2069.
(8) Jia, T. Z.; Chandru, K.; Hongo, Y.; Afrin, R.; Usui, T.; Myojo, K. Membraneless Polyester Microdroplets as Primordial Compartments at the Origins of Life. *Proc. Natl. Acad. Sci. U. S. A.* **2019**, *116*, 15830–15835.
(9) Poudyal, R. R.; Pir Cakmak, F.; Keating, C. D.; Bevilacqua, P. C. Physical Principles and Extant Biology Reveal Roles for RNA-

Containing Membraneless Compartments in Origins of Life Chemistry. *Biochemistry* **2018**, *57*, 2509−2519.
(10) Koga, S.; Williams, D. S.; Perriman, A. W.; Mann, S. Peptide-Nucleotide Microdroplets as a Step towards a Membrane-Free Protocell Model. *Nat. Chem.* **2011**, *3*, 720−724.
(11) Aumiller, W. M.; Pir Cakmak, F.; Davis, B. W.; Keating, C. D. RNA-Based Coacervates as a Model for Membraneless Organelles: Formation, Properties, and Interfacial Liposome Assembly. *Langmuir* **2016**, *32*, 10042−10053.
(12) Drobot, B.; Iglesias-Artola, J. M.; Le Vay, K.; Mayr, V.; Kar, M.; Kreysing, M.; Mutschler, H.; Tang, T. Y. D. Compartmentalised RNA Catalysis in Membrane-Free Coacervate Protocells. *Nat. Commun.* **2018**, *9*, 3643.
(13) Martin, E. W.; Holehouse, A. S.; Peran, I.; Farag, M.; Incicco, J. J.; Bremer, A.; Grace, C. R.; Soranno, A.; Pappu, R. V.; Mittag, T. Valence and Patterning of Aromatic Residues Determine the Phase Behavior of Prion-Like Domains. *Science* **2020**, *367*, 694−699.
(14) Liu, X.; Xie, X.; Du, Z.; Li, B.; Wu, L.; Li, W. Aqueous Self-Assembly of Arginine and K8SiW11O39: Fine-Tuning the Formation of a Coacervate Intended for Sprayable Anticorrosive Coatings. *Soft Matter* **2019**, *15*, 9178−9186.
(15) Frankel, E. A.; Bevilacqua, P. C.; Keating, C. D. Polyamine/Nucleotide Coacervates Provide Strong Compartmentalization of Mg2+, Nucleotides, and RNA. *Langmuir* **2016**, *32*, 2041−2049.
(16) Priftis, D.; Laugel, N.; Tirrell, M. Thermodynamic Characterization of Polypeptide Complex Coacervation. *Langmuir* **2012**, *28*, 15947−15957.
(17) Vieregg, J. R.; Lueckheide, M.; Marciel, A. B.; Leon, L.; Bologna, A. J.; Rivera, J. R.; Tirrell, M. V. Oligonucleotide-Peptide Complexes: Phase Control by Hybridization. *J. Am. Chem. Soc.* **2018**, *140*, 1632−1638.
(18) Shakya, A.; King, J. T. DNA Local-Flexibility-Dependent Assembly of Phase-Separated Liquid Droplets. *Biophys. J.* **2018**, *115*, 1840−1847.
(19) Manning, G. S. The Persistence Length of DNA Is Reached from the Persistence Length of Its Null Isomer through an Internal Electrostatic Stretching Force. *Biophys. J.* **2006**, *91*, 3607−3616.
(20) Onsager, L. The Effects of Shape on the Interaction of Colloidal Particles. *Ann. N. Y. Acad. Sci.* **1949**, *51*, 627−659.
(21) Livolant, F.; Levelut, A. M.; Doucet, J.; Benoit, J. P. The Highly Concentrated Liquid-Crystalline Phase of DNA Is Columnar Hexagonal. *Nature* **1989**, *339*, 724−726.
(22) Nakata, M.; Zanchetta, G.; Chapman, B. D.; Jones, C. D.; Cross, J. O.; Pindak, R.; Bellini, T.; Clark, N. A. End-to-End Stacking and Liquid Crystal Condensation of 6 to 20 Base Pair DNA Duplexes. *Science* **2007**, *318*, 1276−1279.
(23) Zanchetta, G.; Bellini, T.; Nakata, M.; Clark, N. A. Physical Polymerization and Liquid Crystallization of RNA Oligomers. *J. Am. Chem. Soc.* **2008**, *130*, 12864−12865.
(24) Bellini, T.; Zanchetta, G.; Fraccia, T. P.; Cerbino, R.; Tsai, E.; Smith, G. P.; Moran, M. J.; Walba, D. M.; Clark, N. A. Liquid Crystal Self-Assembly of Random- Sequence DNA Oligomers. *Proc. Natl. Acad. Sci. U. S. A.* **2012**, *109*, 1110−1115.
(25) Fraccia, T. P.; Smith, G. P.; Bethge, L.; Zanchetta, G.; Nava, G.; Klussmann, S.; Clark, N. A.; Bellini, T. Liquid Crystal Ordering and Isotropic Gelation in Solutions of Four-Base-Long DNA Oligomers. *ACS Nano* **2016**, *10*, 8508−8516.
(26) Smith, G. P.; Fraccia, T. P.; Todisco, M.; Zanchetta, G.; Zhu, C.; Hayden, E.; Bellini, T.; Clark, N. A. Backbone-Free Duplex-Stacked Monomer Nucleic Acids Exhibiting Watson−Crick Selectivity. *Proc. Natl. Acad. Sci. U. S. A.* **2018**, *115*, E7658−E7664.
(27) Lydon, J. Chromonic Review. *J. Mater. Chem.* **2010**, *20*, 10071−10099.
(28) Rumyantsev, A. M.; De Pablo, J. J. Liquid Crystalline and Isotropic Coacervates of Semiflexible Polyanions and Flexible Polycations. *Macromolecules* **2019**, *52*, 5140−5156.
(29) Bloomfield, V. A. DNA Condensation. *Curr. Opin. Struct. Biol.* **1996**, *6*, 334−341.
(30) DeRouchey, J.; Netz, R. R.; Rädler, J. O. Structural Investigations of DNA-Polycation Complexes. *Eur. Phys. J. E: Soft Matter Biol. Phys.* **2005**, *16*, 17−28.
(31) Zhao, J.; Gulan, U.; Horie, T.; Ohmura, N.; Han, J.; Yang, C.; Kong, J.; Wang, S.; Xu, B. Bin.Advances in Biological Liquid Crystals. *Small* **2019**, *15*, 1900019.
(32) Hamley, I. W. Liquid Crystal Phase Formation by Biopolymers. *Soft Matter* **2010**, *6*, 1863−1871.
(33) Lu, T.; Spruijt, E. Multiphase Complex Coacervate Droplets. *J. Am. Chem. Soc.* **2020**, *142*, 2905−2914.
(34) Todisco, M.; Smith, G. P.; Fraccia, T. P. Liquid Crystal Ordering of DNA Dickerson Dodecamer Duplexes with Different 5 ' -Phosphate Terminations. *Mol. Cryst. Liq. Cryst.* **2019**, *683*, 69−80.
(35) Zanchetta, G.; Giavazzi, F.; Nakata, M.; Buscaglia, M.; Cerbino, R.; Clark, N. A.; Bellini, T. Right-Handed Double-Helix Ultrashort DNA Yields Chiral Nematic Phases with Both Right- and Left-Handed Director Twist. *Proc. Natl. Acad. Sci. U. S. A.* **2010**, *107*, 17497−17502.
(36) Characteristics of Nucleic Acids. *Curr. Protoc. Mol. Biol.* **2004**, *66*, A.1D.1−A.1D.11.
(37) Isom, D. G.; Castañeda, C. A.; Cannon, B. R.; García-Moreno, E. B. Large Shifts in PKa Values of Lysine Residues Buried inside a Protein. *Proc. Natl. Acad. Sci. U. S. A.* **2011**, *108*, 5260−5265.
(38) Perry, S. L.; Li, Y.; Priftis, D.; Leon, L.; Tirrell, M. The Effect of Salt on the Complex Coacervation of Vinyl Polyelectrolytes. *Polymers (Basel, Switz.)* **2014**, *6*, 1756−1772.
(39) Wang, Q.; Schlenoff, J. B. The Polyelectrolyte Complex/Coacervate Continuum. *Macromolecules* **2014**, *47*, 3108−3116.
(40) De Michele, C.; Zanchetta, G.; Bellini, T.; Frezza, E.; Ferrarini, A. Hierarchical Propagation of Chirality through Reversible Polymerization: The Cholesteric Phase of DNA Oligomers. *ACS Macro Lett.* **2016**, *5*, 208−212.
(41) Lucchetti, L.; Fraccia, T. P.; Ciciulla, F.; Bellini, T. Non-Linear Optical Measurement of the Twist Elastic Constant in Thermotropic and DNA Lyotropic Chiral Nematics. *Sci. Rep.* **2017**, *7*, 4959.
(42) De Michele, C.; Bellini, T.; Sciortino, F. Self-Assembly of Bifunctional Patchy Particles with Anisotropic Shape into Polymers Chains: Theory, Simulations, and Experiments. *Macromolecules* **2012**, *45*, 1090−1106.
(43) Di Leo, S.; Todisco, M.; Bellini, T.; Fraccia, T. P. Phase Separations, Liquid Crystal Ordering and Molecular Partitioning in Mixtures of PEG and DNA Oligomers. *Liq. Cryst.* **2018**, *45*, 2306−2318.
(44) Kang, M.; Day, C. A.; Kenworthy, A. K.; DiBenedetto, E. Simplified Equation to Extract Diffusion Coefficients from Confocal FRAP Data. *Traffic* **2012**, *13*, 1589−1600.
(45) Lueckheide, M.; Vieregg, J. R.; Bologna, A. J.; Leon, L.; Tirrell, M. V. Structure-Property Relationships of Oligonucleotide Polyelectrolyte Complex Micelles. *Nano Lett.* **2018**, *18*, 7111−7117.
(46) Oskolkov, N. N.; Potemkin, I. I. Complexation in Asymmetric Solutions of Oppositely Charged Polyelectrolytes: Phase Diagram. *Macromolecules* **2007**, *40*, 8423−8429.
(47) Zhang, P.; Alsaifi, N. M.; Wu, J.; Wang, Z. G. Polyelectrolyte Complex Coacervation: Effects of Concentration Asymmetry. *J. Chem. Phys.* **2018**, *149*, 163303.
(48) Raspaud, E.; Durand, D.; Livolant, F. Interhelical Spacing in Liquid Crystalline Spermine and Spermidine-DNA Precipitates. *Biophys. J.* **2005**, *88*, 392−403.
(49) Liu, G.; Molas, M.; Grossmann, G. A.; Pasumarthy, M.; Perales, J. C.; Cooper, M. J.; Hanson, R. W. Biological Properties of Poly-L-Lysine-DNA Complexes Generated by Cooperative Binding of the Polycation. *J. Biol. Chem.* **2001**, *276*, 34379−34387.
(50) Ziebarth, J.; Wang, Y. Molecular Dynamics Simulations of DNA-Polycation Complex Formation. *Biophys. J.* **2009**, *97*, 1971−1983.
(51) Fraccia, T. P.; Smith, G. P.; Clark, N. A.; Bellini, T. Liquid Crystal Ordering of Four-Base-Long DNA Oligomers with Both G−C and A−T Pairing. *Crystals* **2018**, *8*, 5.

https://dx.doi.org/10.1021/acsnano.0c05083
ACS Nano 2020, 14, 15071−15082

(52) SantaLucia, J.; Hicks, D. The Thermodynamics of DNA Structural Motifs. *Annu. Rev. Biophys. Biomol. Struct.* **2004**, *33*, 415−440.
(53) Rothemund, P. W. K. Folding DNA to Create Nanoscale Shapes and Patterns. *Nature* **2006**, *440*, 297−302.
(54) Pir Cakmak, F.; Choi, S.; Meyer, M. O.; Bevilacqua, P. C.; Keating, C. D. Prebiotically-Relevant Low Polyion Multivalency Can Improve Functionality of Membraneless Compartments. *bioRxiv*, February 25, 2020. DOI: 10.1101/2020.02.23.961920 (accessed March 2, 2020).
(55) Zanchetta, G.; Nakata, M.; Buscaglia, M.; Bellini, T.; Clark, N. A. Phase Separation and Liquid Crystallization of Complementary Sequences in Mixtures of NanoDNA Oligomers. *Proc. Natl. Acad. Sci. U. S. A.* **2008**, *105*, 1111−1117.
(56) Theis, J. G.; Smith, G. P.; Yi, Y.; Walba, D. M.; Clark, N. A. Liquid Crystal Phase Behavior of a DNA Dodecamer and the Chromonic Dye Sunset Yellow. *Phys. Rev. E: Stat. Phys., Plasmas, Fluids, Relat. Interdiscip. Top.* **2018**, *98*, 042701.
(57) Poudyal, R. R.; Guth-metzler, R. M.; Veenis, A. J.; Frankel, E. A.; Keating, C. D.; Bevilacqua, P. C. Template-Directed RNA Polymerization and Enhanced Ribozyme Catalysis inside Membraneless Compartments Formed by Coacervates. *Nat. Commun.* **2019**, *10*, 490.
(58) Martin, N.; Tian, L.; Spencer, D.; Coutable-Pennarun, A.; Anderson, J. L. R.; Mann, S. Photoswitchable Phase Separation and Oligonucleotide Trafficking in DNA Coacervate Microdroplets. *Angew. Chem., Int. Ed.* **2019**, *58*, 14594−14598.
(59) Fraccia, T. P.; Smith, G. P.; Zanchetta, G.; Paraboschi, E.; Yi, Y.; Yi, Y.; Walba, D. M.; Dieci, G.; Clark, N. A.; Bellini, T. Abiotic Ligation of DNA Oligomers Templated by Their Liquid Crystal Ordering. *Nat. Commun.* **2015**, *6*, 6424.
(60) Todisco, M.; Fraccia, T. P.; Smith, G. P.; Corno, A.; Bethge, L.; Klussmann, S.; Paraboschi, E. M.; Asselta, R.; Colombo, D.; Zanchetta, G.; Clark, N. A.; Bellini, T. Nonenzymatic Polymerization into Long Linear RNA Templated by Liquid Crystal Self-Assembly. *ACS Nano* **2018**, *12*, 9750−9762.
(61) Szostak, J. W. The Eightfold Path to Non-Enzymatic RNA Replication. *J. Syst. Chem.* **2012**, *3*, 2.
(62) Frenkel-Pinter, M.; Samanta, M.; Ashkenasy, G.; Leman, L. J. Prebiotic Peptides: Molecular Hubs in the Origin of Life. *Chem. Rev.* **2020**, *120*, 4707−4765.
(63) Mulkidjanian, A. Y.; Bychkov, A. Y.; Dibrova, D. V.; Galperin, M. Y.; Koonin, E. V. Origin of First Cells at Terrestrial, Anoxic Geothermal Fields. *Proc. Natl. Acad. Sci. U. S. A.* **2012**, *109*, E821−E830.
(64) Damer, B.; Deamer, D. The Hot Spring Hypothesis for an Origin of Life. *Astrobiology* **2020**, *20*, 429−452.
(65) Doostmohammadi, A.; Ignés-Mullol, J.; Yeomans, J. M.; Sagués, F. Active Nematics. *Nat. Commun.* **2018**, *9*, 3246.
(66) Lydon, J. Microtubules: Nature's Smartest Mesogens — A Liquid Crystal Model for Cell Division. *Liq. Cryst. Today* **2006**, *15*, 1−10.

https://dx.doi.org/10.1021/acsnano.0c05083
ACS Nano 2020, 14, 15071−15082